OFFICE OF NAVAL RESEARCH
CONTRACT N6 onr-27015

# MODEL STUDY OF DYNAMIC STABILITY OF HELICOPTERS PHASE I DEVELOPMENT OF MODEL & TESTING TECHNIQUES

By

R. B. GRAY, A. M. McCASKILL, A. A. NIKOLSKY,
A. K. POOLE and S. E. SLAYMAKER



PRINCETON UNIVERSITY

AERONAUTICAL ENGINEERING LABORATORY

Report No. 190

# DISCLAIMER NOTICE

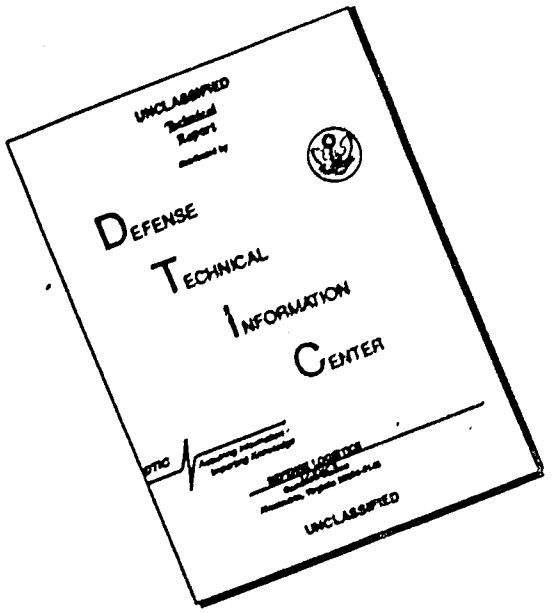


THIS DOCUMENT IS BEST QUALITY AVAILABLE. THE COPY FURNISHED TO DTIC CONTAINED A SIGNIFICANT NUMBER OF PAGES WHICH DO NOT REPRODUCE LEGIBLY.

[redacted]



OFFICE OF NAVAL RESEARCH

CONTRACT N6onr-27015

FEBRUARY 1, 1952

REPORT NO. 190

# MODEL STUDY OF DYNAMIC STABILITY OF HELICOPTERS

## PHASE I

## DEVELOPMENT OF MODEL AND TESTING TECHNIQUES

Prepared by:

Robin B. Gray
Research Assistant

Allan M. McCaskill
Research Assistant

Allan K. Poole
Research Assistant

S. E. Slaymaker
Research Associate

Approved:

A. A. Nikolsky
Project Supervisor



[redacted]

# MODEL STUDY OF DYNAMIC STABILITY OF HELICOPTERS

## PHASE I

## DEVELOPMENT OF MODEL AND TESTING TECHNIQUES


### SUMMARY

This report represents the successful conclusion and presents the results of Phase I of a general experimental investigation of hovering stability of a two-dimensional model helicopter from which all lateral motion has been eliminated except that of the stabilizer bar and tip path plane. The sole objective of this first phase was the development of the test facility, the model, its instrumentation, and the completion and partial reduction of data for one test run. Therefore, this report deals primarily with a description of the test facility and model and includes a discussion of the reasons for and validity of the test method herein described.

The model's hovering performance, as determined from thrust stand data, is included in graphical form, as are the experimental results of the test run. The theoretical performance of the model after a slight disturbance from hovering flight has been calculated for both a stable configuration and a stability boundary configuration, and is also graphically presented herein.

This investigation was carried out at Princeton University under the sponsorship of the Office of Naval Research and with the financial assistance of the Bureau of Aeronautics.


### INTRODUCTION

With the increasing usefulness of rotary wing aircraft for both military and civilian application, it has become apparent that methods must be developed for accurately predicting their stability characteristics. The primary purpose of an investigation along these lines would be the determination of the static and dynamic stability derivatives. Theoretical analyses have been made of the stability and control characteristics of a helicopter slightly disturbed from hovering flight, and theoretical methods of determining stability derivatives have been arrived at. (References 1, 2, and 3.) However these theories cannot be used with confidence until the values of the theoretically derived stability derivatives have either been verified

experimentally or replaced by empirical values determined from experiment. Such an experimental investigation would also prove or disprove the validity of certain simplifying assumptions made in the theory, and, if the latter were so, it would show the way for improvement.

A broad experimental program has been undertaken to determine the stability derivatives of a model helicopter near hovering flight. This program has been divided into several phases. Phase I, of about one year's duration and described herein, was concerned with the development of the test facility, design and construction of the model system and its instrumentation, and the development of testing techniques. A theoretical analysis of the model using existing theory was made, but no comparison of theory with experiment was attempted nor extensive experimental data recorded.

Phase II, which is now under way, is concerned with the measurement, recording, and reduction of flight data with the model in several stable and unstable configurations. The various dynamic stability derivatives will be calculated from the experimental data, non-dimensionalized, and a comparison made with the theoretical derivatives. An attempt will be made to adjust the theory either theoretically or by the inclusion of empirical stability derivatives to allow for any discrepancies that may be discovered. The stability characteristics of the model will then be calculated for a flight condition different from any previous ones and checked experimentally. This phase will also be of approximately one year's duration.

A possible extension of the program would be an investigation of the effect of blade flexibility on dynamic stability derivatives of a model helicopter near hovering flight. The next step might possibly be that of entering the forward flight regime. This would require not only the measurement of dynamic stability derivatives, but also the determination of the static stability derivatives, either from wind tunnel tests or from actual steady forward flight along the track.

The practicability of modifying the methods and apparatus of the present phase for forward flight stability tests is currently being investigated.

SYMBOLS

Physical Quantities

| | |
|---|---|
| $W_z$ | Lifting weight of model, pounds |
| $W_x$ | Horizontal traveling weight of model, pounds (model plus carriage and portion of trailing cable) |
| b | Number of blades |
| R | Blade radius, feet |
| c | Blade-section chord, feet |
| $\sigma$ | Rotor solidity $\frac{bc}{\pi R}$ |
| $\theta_o$ | blade pitch angle at hub, radians |
| $B_{l_c}$ | Longitudinal cyclic blade pitch angle variation at hub; cyclic input disturbance: pilot's control term, radians |
| $B_l$ | Total longitudinal cyclic blade pitch angle variation at hub |
| m | Mass of blade per foot of radius, slugs per foot |
| $I_l$ | Mass moment of inertia of rotor about flapping hinge, lb-ft-sec$^2$. |
| $\alpha_l$ | Longitudinal fuselage attitude angle, angle between plane perperdicular to rotor shaft and horizontal reference plane, radians |
| $\bar{\lambda}$ | Damping factor, indicates rate of increase or decrease of model motion, seconds$^{-1}$ |
| h | Distance along shaft axis from rotor hub to model center of gravity feet |
| $I_{yo}$ | Model mass moment of inertia less blades about lateral axis through center of gravity, lb-ft-sec$^2$. |
| $I_{lb}$ | Mass moment of inertia of stabilizer bar about its pivoting axis, lb-ft-sec$^2$. |
| $\kappa$ | Viscous damping coefficient applied to bar, ft-lb per radian per second |
| $\bar{c}$ | ratio of viscous damping coefficient to moment of inertia of bar, seconds$^{-1}$. |

$K$ Linkage ratio between bar and blade feathering motion.

$t$ Time, seconds.

$\beta_o$ Built in coning angle of blades, radians

Air-Flow Parameters:

$V_z$ Vertical component of true airspeed of model, feet per second

$V_x$ Horizontal component of true airspeed of model, feet per second

$\Omega$ Rotor angular velocity, radians per second

$a_1$ Longitudinal rotor angle of attack, angle between tip path plane and direction of flight path, radians

$\mu_x$ Horizontal tip-speed ratio $(\frac{V_x}{\Omega R})$

$\Psi$ Blade azimuth angle measured from downwind position in direction of rotation $(\Omega t)$, radians

Aerodynamic Characteristics:

Blade-element aerodynamic characteristics

$c_l$ Section lift coefficient

$c_{d_o}$ Section profile-drag coefficient

$\delta$ Mean profile drag coefficient

$a$ Slope of curve of section lift coefficient against section angle of attack (radian measure)

Rotor aerodynamic characteristics

$L$ Lift, pounds

$T$ Rotor thrust, pounds

$Q$ Rotor-shaft torque, pound-feet

$C_T$ Thrust coefficient $\frac{T}{\pi R^2 \rho (\Omega R)^2}$

$C_Q$ Rotor-shaft torque coefficient $\frac{Q}{\pi R^2 \rho (\Omega R)^2 R}$

## DESCRIPTION OF APPARATUS

### Test Facility

The test facility is comprised of a brick building 28 feet wide and 58 feet long, whose lateral cross-section is as shown in figure 1, and a control room as also shown in figure 1. The control room is built into the side of the building and affords complete protection for test personnel, controls, and recording equipment. Test personnel have an unobstructed view of the model in any position on the track, the model being viewed through one-half inch thick plexiglas.

The tracks are mounted on a cinder block wall at a height of four and one quarter feet above the lower level of the building. The track system is built up of extruded aluminum channel and "T" sections as shown in figure 2, and is so designed that both vertical and horizontal adjustments for alignment may be made by means of screws.

### Model Supporting Structure

The carriage is constructed of 24 ST extruded aluminum angle sections. It rolls on and is held on the track by means of four pair of ball bearing rollers. One of each pair runs on top of the track, the other mounted directly below the first runs on the underside of the track. The carriage is centered on the track by means of four additional bearings which roll against the inside edge of the track. (See figure 3) The chassis of the carriage is of rectangular shape, the bearings being mounted at each corner.

Vertical freedom of motion is accomplished by allowing a square aluminum tube to move freely on four pair of ball bearing rollers which are mounted on the superstructure of the carriage, and are arranged about the tube as shown in figure 4, with two pair to each set and a distance between sets of seven inches. Positive stops are built into each end of the square tube. On the upper end of the tube is mounted a yoke, also constructed of aluminum, which carries the bearings supporting the trunnions about which the model is free to pitch. Pitch stops are attached to the yoke which limit the model pitch angle to thirty degrees in either direction. Lateral and rolling motions are completely eliminated.

Model

The model itself is mounted in the yoke so that the pitch axis passes through the center of gravity of the model. Power is supplied by a heavy-duty disc sander type motor which develops about one and one-half horsepower when run at a stepped-up voltage. The motor as well as all the component parts of the model are shown in figure 5.

The motor is geared to the rotor shaft through a two-stage planetary gear system allowing a 12 to 1 speed reduction. The first stage planetary gear and the second stage sun gear are shown in figure 6 mounted on the motor with the gear box containing the ring gears at one side. Figure 7 shows the gear box in place with the second stage planetary gear shown mounted on the rotor shaft in the foreground. All gears are splash lubricated with a medium light weight motor oil. Figure 8 shows the rotor shaft in place as well as the six slip-rings required for the rotor tilt angle and stabilizer bar tilt angle indicating circuits.

Figure 9 shows the installation of the magnetic clutches. To one side is shown the clutch housing which carries the follow-up potentiometers and the brushes for the slip rings. In the foreground are the screw-jacks. The lower side of each magnetic clutch is geared directly to the rotor shaft. The other side of each pair is geared directly to a screw jack comprising the lower end of the corresponding blade linkage system and to a follow-up potentiometer. Figure 10 shows the clutch housing in place with the follow-up potentiometer and the screw jacks installed. The control for each pair of magnetic clutches is an identical potentiometer mounted in the control room. The two potentiometers of each control are so connected electrically that a movement of the control potentiometer introduces an error signal in the electrical system which by means of an electronic amplifier causes one of the pair of magnetic clutches to engage, thus running the screw jack up or down and rotating the follow-up potentiometer so as to cancel out the error signal and stop the motion. This introduces the desired control motion to the model.

In the foreground of figure 10 are shown the cover plate of the clutch housing and the swash plate assembly. Figure 11 shows these components in their installed position. The screw jack on the right engages the collective linkage; that on the left, the cyclic. The swash-plate may be tilted only about an axis parallel to the model pitch axis. The scissors levers are shown attached to the swash plate by the monkey links and pivoted on the collective pitch sleeve. Vertical movement of the sleeve introduces an equal angle to each blade by means of linkages, tilt of the swash plate introduces a cyclically varying angle.

In the foreground of figure 11 are shown from left to right: the stabilizer bar damping pot, a micro-torque potentiometer for indicating bar tilt, the stabilizer bar with mixing levers and connecting links, the blade hub, and the potentiometer for indicating rotor plane tilt. These components are shown installed in figures 12 and 13. Also shown in figure 12 are the magnetic clutch amplifiers, the control box, and the rotor blades. As may be seen, the lifting rotor has two blades which are connected to each other rigidly and to the shaft by means of a universal joint. The rotor blades are constructed of solid spruce with a one-eighth inch by three-eighths inch strip of brass buried in the leading edge so that they are balanced about their quarter chord which is also their feathering axis. The airfoil section is a NACA 0015. The blade surface has a smooth lacquered finish.

The stabilizer bar as shown in figures 11, 12, and 13 is the Bell type and consists of a bar with a mass on either end connected at its center by a pivot to the shaft at a point below the rotor plane and at right angles to the feathering axis of the blades. The bar is further connected by suitable linkages to the blades and is free to pivot up and down while rotating. This "see-saw" motion is provided with viscous damping which determines the rate at which the motion of the bar follows the disturbed angular motion of the model shaft. The motion of the bar may introduce a cyclic variation in rotor blade angle by means of the aforementioned linkages. Thus while the model is hovering, the bar is rotating in a plane perpendicular to the rotor shaft and the rotor blade angle is not affected. However, if the model is disturbed in pitch, the bar, due to gyroscopic forces, tends to remain parallel to its original plane of rotation, and hence introduces automatically a cyclic variation in blade pitch angle which tends to restore the model to its hovering condition. The main factors which affect this automatic stabilization are the viscous damping applied to the bar and the linkage ratio between the bar and the rotor.

Viscous damping is applied to the stabilizer bar by means of a solid "swinging gate" immersed in a hemi-cylinder of hydraulic fluid and pivoted about the axis of the cylinder. The portions of hydraulic fluid separated by the gate are connected through a passage and an adjustable needle valve. The pivot shaft of the gate is geared directly to the bar and is free to pivot as the bar does. When the model is disturbed, the bar begins to rock back and forth as stated before. This movement forces the hydraulic fluid through the needle valve and results in the application of a viscous restraint to the bar. Different values of damping may be realized by adjusting the needle valve.

To change the linkage ratio between the bar and the rotor requires a different set of mixing levers, and associated links.

Vertical and horizontal motions are limited by the engagement of elastic shock cord by the model and carriage, which gives adequate protection to the model when and if control is lost.

## INSTRUMENTATION

The model and carriage are instrumented to record the following data: vertical and horizontal displacements, vertical and horizontal acceleration, fuselage attitude angle, stabilizer bar tilt angle with respect to rotor shaft, rotor tilt angle with respect to rotor shaft, collective blade pitch angle, cyclic blade pitch angle, and rotor shaft speed. It has been planned to add an angular accelerometer to measure fuselage attitude accelerations before Phase II is begun.

Vertical and horizontal displacements are recorded by means of a series of electrical contacts mounted on the track and on the square tube. As the model moves vertically or horizontally, insulated leaf springs mounted on the carriage brush these contacts and close the circuit, thus allowing an electrical pulse to flow in the circuit which may be recorded by an oscillograph. The amplitude and polarity of the pulse vary from contact to contact in a pre-set manner so that they form a pattern on the oscillograph record. A reversal of direction reverses the order in which the contacts are made, and hence the pattern on the record, which allows easy identification of reversal in direction and displacement at which it occurs.

A miniature accelerometer of range $\pm$ 1.5g is mounted on the vertical tube to generate a signal for the recording of vertical accelerations. A similar accelerometer is mounted on the carriage for horizontal accelerations.

Fuselage attitude angle is recorded by means of a potentiometer which is driven by a spur gear mounted on the model pitch shaft. The potentiometer has a voltage impressed across its outside terminals. The center terminal is grounded; one of the outer terminals is led to the oscillograph where a rotation of the potentiometer shaft is recorded as a galvanometer deflection. Both bar tilt and rotor plane tilt are recorded in a similar manner. An angular accelerometer is to be mounted on the fuselage pitch axis to measure fuselage attitude angular accelerations.

Collective and cyclic blade pitch angle are recorded as an oscillograph galvanometer deflection proportional to the change in resistance from the center terminal to an outside terminal of their respective follow-up potentiometers.

Rotor shaft speed is obtained by recording an electrical pulse introduced by the opening of a set of breaker points by a cam mounted on the rotor shaft.

A visual indication of rotor speed is obtained for the operator by measuring the output voltage of a small d.c. generator mounted on the bottom of the motor case and driven at motor shaft speed.

This comprises the instrumentation anticipated for the successful measurement of flight data.

All data are recorded by a Heiland Type A 301R Oscillograph.

## TEST PROCEDURE

A typical run is as follows: First the bar damping is set at the desired value. Then the model is brought up to speed and made to hover at one end of the track. When the model is in steady hovering flight, the recording circuits and oscillograph are turned on and a given disturbance is applied to the rotor by introducing an error signal into the cyclic pitch circuits. An oscillograph record is taken of the subsequent motion until the flight is completed or until the model engages one of the stops. The oscillograph record is then developed, and the data analysis begun.

Since most of the data is recorded as a resistance measurement depending on an impressed voltage, the affected components are calibrated before and after each day's tests so that proper allowance may be made for a drop in voltage as the batteries are used.

## PRECISION

It is conservatively estimated that the measured and recorded data will have the following tolerances--

| | |
|---|---|
| Angular measurements | ± 1/4 ° |
| Linear measurements | ± 1/32 in. |
| Rotor shaft speed | ± 20 RPM |
| Accelerations | ± 0.02 g |

## RESULTS

The results of the model and test facility development are presented in the main, pictorially. Figure 14 shows the model, supporting members, and carriage mounted on the track. In the foreground are strands of elastic shock cord stretched across the track to snub the model. The cable carrying the power, control, and position indicator circuits is shown, trailing to the left of the model.

Figure 15 is a closer view of the model showing the method of attachment to the yoke and carriage. Figure 16 is a general view of the laboratory, with the control room on the left. Figure 17 is a broadside view of the control room with the model and tracks in the foreground. In figure 18, a close-up of the control room is shown and the general arrangement of controls and recording apparatus is indicated.

The experimental results of a thorough static thrust analysis are presented graphically in figures 19, 20, and 21. Figure 19 is a plot of thrust coefficient versus blade pitch angle and a comparison with theory for a lift curve slope of 5.75 per radian. Figure 20 is a plot of the torque coefficient-thrust coefficient polar, and figure 21 shows the variation of rotor profile drag coefficient with blade pitch angle for a 3/4 radius Reynolds Number of 313,000. Table I lists the measured model characteristics.

Figure 22 shows that the variation in stabilizer bar damping as determined statically by experiment is linear with speed and that the damping coefficient is therefore constant for a given needle valve setting.

A sample oscillograph record is presented as figure 23 to show the present status of the recording circuits. Data from this record are presented in figures 24 and 25. Figure 24 shows a typical fuselage attitude versus time record whose half period is 3.4 seconds with a computed damping factor of $-.454\ sec^{-1}$ for a cyclic blade pitch disturbance of 3.0 degrees. Presented in figure 25 is the horizontal velocity response whose half period is 4.75 seconds with a computed damping factor of $-.459\ sec^{-1}$. Collective blade pitch angle was measured and found to be 11.0 degrees. Other data was not reduced, either because it is not of much interest at this time or because of obvious reduction difficulties whose elimination will be discussed later. Table II lists the calibration constants for the oscillograph galvanometer deflections.

Theoretical responses of the model, using the theory of Appendix 1, for two values of stabilizer bar damping were computed and presented as figures 26, 27, and 28. Figures 26 and 27 show the horizontal velocity response and figure 28 shows the fuselage attitude response of the model for a given assumed cyclic blade pitch disturbance.

## ANALYSIS

The dynamic stability characteristics of the model are determined from its motion following a disturbance from steady hovering flight. The various oscillatory motions of the model are assumed to be of the form

$$N = N_o e^{\bar{\lambda} t} \cos \omega t$$

where N is the amplitude of the disturbed motion, $\bar{\lambda}$ is the damping factor, and $\omega$ is the frequency of oscillation. Obviously, the product $N_o e^{\bar{\lambda} t}$ defines the envelope of the resulting motion and $\bar{\lambda}$ gives the characteristics of the dynamic stability; that is, both the degree and type of damping present. Solving the above equation for $\bar{\lambda}$ and remembering that only the maximum amplitude is necessary so that $\cos \omega t = \pm 1$, yields

$$\bar{\lambda} = \frac{\ln N_2 - \ln N_1}{t_2 - t_1}$$

where $N_2$ and $N_1$ are two successive maximum amplitudes occurring at time $t_2$ and $t_1$. Thus the stability characteristics may be determined directly from the oscillograph record, by measuring the galvanometer deflection at two successive peaks, noting the difference in time between the two peaks, and substituting these values in the above equation. The period of the oscillation may be determined by measuring the time required for a complete oscillation as indicated on the oscillograph trace.

Vertical and horizontal velocities are determined from the slopes of the displacement versus time plots.

Vertical forces, horizontal forces, and fuselage pitching moments are determined by the application of Newton's First and Second Laws to the observed motion. Since the accelerations are measured and all remaining physical quantities are known, the calculation of these quantities is a simple

matter. If these forces are then plotted versus various parameters, the slope of the curve as it passes through zero gives the desired dynamic stability derivatives. These derivatives are then compared with the theoretical ones derived in chapter 6 of reference 1.

## DISCUSSION

This investigation has been concerned with the development of a model helicopter and testing techniques suitable for the further study of the dynamic stability characteristics of rotary wing aircraft. The method herein described was chosen for its apparent simplicity and adaptability to easy construction and instrumentation. It is easy to see that the elimination of all lateral motion except that of the stabilizer bar and rotor has greatly simplified the problem. Physically this results in the model's being a representation of one rotor of a twin-rotor helicopter with side by side, oppositely rotating rotors, because any longitudinal motion causes equal and opposite lateral inclinations of the two tip path planes which results in a cancellation of lateral forces. The end result being that no lateral motion ensues. Since the theory was developed with this in mind, a direct valid comparison may be made between experimental and theoretical dynamic stability derivatives. It is also obvious that the stability derivatives, due to their nature, will also be applicable to a single-rotor helicopter for motion near hovering flight.

The presence of the carriage, i.e., the fact that the traveling weight is different from the lifting weight, has been accounted for in the theoretical analysis and should have absolutely no effect on the comparison of stability derivatives.

The effect of the bearing friction is quite small, as is adequately evidenced by the ease with which a slight push will start the carriage and model moving along the track. Its subsequent coasting ability is quite good.

The effect of the trailing cable appears to be quite large at present. The next step in reducing its effect will be the replacement of the present bundle of wires with a single, multi-conductor cable of much lighter weight and smaller dimensions. If this should still appear to have a prohibitive effect, the trailing cable system will be eliminated and a series of third rails will be installed. However, if the effect of the new trailing cable appears small, it may also be adequately accounted for in the theoretical analysis, or even completely neglected.

It is quite apparent that since the rotor blades are considerably stiffer, relatively, than those of a full scale helicopter, the effect of blade flexibility should be small.

The handling qualities of the model are comparatively good. It is quite sensitive to control movement, and the magnetic servo clutch system is operating satisfactorily. The model may be flown "hands off" for a considerable length of time. A novice "pilot" can learn to fly it safely in a surprisingly short period of time.

At present, the model is about three pounds overweight, which requires a much larger blade pitch angle and rotor RPM than was originally contemplated. An investigation is now under way to determine the possibility of replacing the present motor with a 400 cycle aircraft hydraulic pump motor of about half the weight of the present motor and capable of developing two horsepower continuously. It appears that this conversion may be made with a minimum of design changes. The main advantage of such a conversion lies in the weight saving which results in a reduction of the blade pitch angle and rotor RPM required. This weight reduction also will allow the installation of an angular accelerometer on the fuselage pitch axis. It is estimated that the resulting lifting weight will be less than 29 pounds, a considerable reduction.

Figures 19, 20, and 21 give the results of a static test analysis of the model. As may be seen from figure 19, the comparison of experiment with theory is quite good for a lift curve slope of 5.75 per radian. Rotor profile drag coefficient versus blade angle was determined from thrust stand data and plotted in figure 21. The value of this coefficient is required for the theoretical analysis, it being primarily a Reynolds Number correction.

A sample oscillograph record is presented in figure 23. As may be seen, all traces are satisfactory except those indicating the rotor tilt angle and the two components of acceleration. As yet, the reason for the "hash" in the rotor tilt angle has not been determined, but is is thought to be mechanical and capable of being eliminated as it does not appear in some of the first records taken. The principal culprit causing the "hash" in the vertical acceleration is the amplifier for the cyclic pitch magnetic clutches. This may be eliminated simply by shielding the leads which will be done when the new trailing cable is installed. It would appear, though, from the horizontal acceleration, that some residual hash will be left in the vertical trace. There are two avenues open for elimination of this in both traces, since it appears to be due primarily to vibration of the model and carriage. One would be to use a properly designed filter in the circuit, the other would be to increase the galvanometer damping. One or the other method will be attempted.

As may be seen from the record, the stabilizer bar is not working properly because there should obviously be a continued oscillation of the bar since the fuselage attitude is continually changing. The reason that it is not working properly is that the control forces due to centrifugal blade feathering appear to be much larger than the gyroscopic forces and the effect of this is essentially to lock the bar to the shaft except when a cyclic pitch variation is impressed. This may be easily remedied by increasing the inertia of the bar until it is large compared to the control forces.

Further evidence that the oscillograph record is satisfactory is presented in figures 24 and 25 which show the fuselage attitude response and horizontal velocity response of the model for the shown cyclic input disturbance. The fact that a stable motion has resulted, whereas it would be expected that the model would be unstable since the stabilizer bar is inoperative, is thought to be a direct result of the trailing cable.

Several theoretical responses of the model have been calculated and are presented as figures 26, 27, and 28 to show what may be predicted for arbitrary values of stabilizer bar damping coefficient. No comparison with experimental results is attempted nor intended. Figure 27 shows that, theoretically, the complete motion of a stable model may be recorded on the track available for any impulse cyclic input disturbance of less than about 2 1/2°. It is therefore anticipated that satisfactory data may be recorded for both stable and unstable models simply by keeping the cyclic input disturbance small enough.

There appears to be a slight recirculation effect when the model is hovered at low altitude and near the ends of the building, which is indicated by an unsteadiness of the model. However, when the model is hovered in a normal flight position and at a short distance from the ends of the building, this effect seems to become negligible.

## CONCLUSIONS

With the completion of the minor adjustments and modifications indicated in the discussion, the model and recording equipment will be ready to begin Phase II, the recording of the disturbed motion of the model and the calculation and comparison of the dynamic stability derivatives.

Princeton University
Princeton, N. J., January 25, 1952

# APPENDIX

## THEORETICAL ANALYSIS

The theory which is used in this investigation of the dynamic stability of a helicopter near hovering flight is identical with that derived in Chapters 5 and 6 of reference 1, except for a few minor modifications of terms as indicated below.

The modifications to the theory of reference 1 are the inclusion of the effect of the stabilizer bar on the blade pitch angle and the redefinition of terms to account for a see-saw type rotor. The bar introduces a cyclic variation in blade pitch angle which is brought about by the motion of certain linkages inserted in the pitch change mechanism for the purpose of following the motion of the bar, whose tendency is to remain in the initial phase of rotation. The movement of the bar out of this initial plane of rotation is a direct function of the damping built into the system and of the friction in the linkages. The effect of the bar on the blade pitch angle may be derived from the equation of motion of the bar.

The equation of motion of the bar may be obtained by writing the equation of moment equilibrium about its rocking hinge. Thus

$$(M_y)_{mb} + (M_y)_{db} + (M_y)_{fb} = 0$$

where

$(M_y)_{mb}$ = the moment due to inertia loads on the bar

$(M_y)_{db}$ = the moment due to a viscous restraint between the frame of the helicopter and the bar

$(M_y)_{fb}$ = the moment of all forces acting on the blade about its feathering axis (assumed to be small in comparison and hence neglected).

Expressing $\beta_b$, the angle between the horizontal reference plane and the axis of the bar, as

$$\beta_b = -a_{1b} \cos \Psi - b_{1b} \sin \Psi$$

where $a_{1b}$ and $b_{1b}$ are positive when the bar is tilted away from the direction of motion and the advancing blade, the moment due to inertia loads becomes, in a manner similar to equation 6.13a, reference 1,

$$-\frac{(M_y)_{mb}}{I_{1b}} = (2\dot{a}_{1b}\Omega - \ddot{b}_{1b}) \sin \Omega t - (2\dot{b}_{1b}\Omega + \ddot{a}_{1b}) \cos \Omega t$$

where

$I_{1b}$ = the moment of inertia of the bar about its rocking hinge

$\Omega$ = rotational velocity of rotor and bar.

The angle $\alpha_b$, between the plane perpendicular to the shaft and the plane of the bar is

$$\alpha_b = \beta_b - \alpha$$

where

$\alpha$ = the angle between the horizontal reference plane and the plane perpendicular to the shaft.

The angle $\alpha$, may be expressed as

$$\alpha = \alpha_1 \cos \Omega t + \alpha_2 \sin \Omega t$$

and since $\alpha_2$ is being maintained equal to zero by means of mechanical restraints in this investigation, the angle $\alpha_b$ may be expressed as

$$\alpha_b = -(\alpha_1 + a_{1b}) \cos \Omega t - b_{1b} \sin \Omega t$$

Therefore, the moment due to a viscous restraint between the frame of the helicopter and the bar becomes

$$(M_y)_{db} = c\,\dot{\alpha}_b$$

$$= c\{[-(\dot{\alpha}_1 + \dot{a}_{1b}) - b_{1b}\Omega]\cos\Omega t - [\dot{b}_{1b} - \Omega(\alpha_1 + a_{1b})]\sin\Omega t\}$$

where

$c$ = viscous restraint and is assumed negative

$\dot{\alpha}_b = \frac{d\alpha_b}{dt}$

Equating the coefficients of similar trigonometric functions contained in the two moment equations results in two differential equations. Then taking the Laplace transform of these two equations and setting the initial conditions equal to zero results in the following expression

$$\frac{\alpha_1 + a_{1b}}{\alpha_1} = \frac{-\lambda^2(\lambda^2 - \bar{c}\lambda) - 2\lambda\Omega^2(2\lambda - \bar{c})}{-\Omega^2(2\lambda - \bar{c})^2 + (\lambda^2 - \bar{c}\lambda)^2}$$

where

$\lambda$ = Laplace transform variable

$\bar{c} = \frac{c}{I_{1b}}$

Following Miller's suggestion, reference 2, that only the effect of the stabilizer bar on small roots is of interest, the assumptions may be made that $\lambda$ is small by comparison with $\Omega$ and hence

$$\frac{\alpha_1 + a_{1b}}{\alpha_1} = \frac{2\lambda}{2\lambda - \bar{c}}$$

As previously pointed out, the motion of the bar automatically causes a cyclic variation in blade pitch angle which is directly proportional to this motion due to the manner in which the blade feathering mechanism is linked to the bar. Since the bar is 90° out of phase with the blades, this blade pitch change is

$$\theta = K[-b_{1b} \cos \Omega t + (a_1 + a_{1b}) \sin \Omega t]$$

where

K = the gear ratio between bar and blade feathering axis.

Since the model is restrained to motion in one plane, only the coefficient of sin $\Omega t$ is of interest, as this is the term which tilts the rotor plane and hence the whole model about the lateral axis. The neglect of the cos $\Omega t$ term results in a small error in the longitudinal response as it was shown in reference 2 that the effect of the lateral response on the longitudinal response may be neglected. Therefore the expression for the total control angle may be written in the form

$$B_1 = B_{1c} - \frac{2\lambda K a_1}{2\lambda - \bar{c}}$$

where $B_{1c}$ is the pilot's control term.

The applicable equations of motion are equations 6.32d and 6.33d on page 220 of reference 1 and the following equation which has been modified for see-saw blades and is to be substituted for equation 6.31d of the same page and reference.

$$\mu_x(\lambda)B_{31} + \alpha_1(\lambda)B_{32} + a_1(\lambda)B_{33} = (\mu_x)_0 P'_{31} + [(\dot{\alpha}_1)_0 \lambda] P'_{32}$$
$$+ [(\dot{a}_1)_0 \lambda + (a_1)_0 \lambda^2] N'_{33} + (a_1)_0 P'_{33}\lambda + (2\lambda - \bar{c})\mathcal{L} B_{1c}$$

where

$$B_{31} = 2\lambda M'_{y_{\mu_x}} - \bar{c} M'_{y_{\mu_x}} = P'_{31}\lambda + Q'_{31}$$

$$B_{32} = -2\lambda(1+K) + \bar{c} = P'_{32}\lambda + Q'_{32}$$

$$B_{33} = 2M'_{y_{\dot{a}_1}} \lambda^2 - \lambda(2 + \bar{c} M'_{y_{\dot{a}_1}}) + \bar{c} = N'_{33}\lambda^2 + P'_{33}\lambda + Q'_{33}$$

and the various terms are as defined in reference 1 except that $I_1$, wherever it appears is now equal to the moment of inertia of two blades and $\beta_0$ is the built in coning angle of the blades.

## REFERENCES

1. Nikolsky, A. A. Helicopter Analysis. John Wiley and Sons, Inc., 1951.

2. Miller, R. H., "Helicopter Control and Stability in Hovering Flight," J. Aeronaut. Sci., August 1948.

3. Miller, R. H., "A Method for Improving the Inherent Stability of Helicopters," J. Aeronaut. Sci., June 1950.

# TABLE I

## MEASURED MODEL CHARACTERISTICS

Rotor:

No. of blades, b = 2
Blade radius, R = 3 feet
Solidity, $\sigma$ = .0441
Blade chord, c = 0.208 feet
Blade airfoil section - NACA 0015
Slope of lift curve, a = 5.75/radian
Moment of inertia, $I_1$ = .160 lb-ft-sec$^2$
Preconing angle, $\beta_o$ = .0436 radians

Weights:

Lifting weight, $W_z$ = 32 lbs.
Total traveling weight, $W_x$ = 43 lbs.
Model center of gravity position: h = 1.013 ft below rotor hub and on rotor shaft axis
Model mass moment of inertia less blades, $I_{y_o}$ = 0.194 lb-ft-sec$^2$

Stabilizing Bar:

Mass moment of inertia, $I_{lb}$ = 0.00557 lb-ft-sec$^2$
Linkage ratio, K = -0.60

TABLE II

CALIBRATION CONSTANTS FOR THE OSCILLOGRAPH GALVANOMETER DEFLECTIONS

| | |
|---|---|
| Collective blade pitch angle | 12.18°/in. |
| Cyclic blade pitch angle | 13.52°/in. |
| Rotor tilt angle with respect to shaft | 11.23°/in. |
| Stabilizer bar tilt with respect to shaft | 24.15°/in. |
| Fuselage tilt angle with respect to horizontal | 25.00°/in. |
| Vertical displacement between impulses | 1.00 in. |
| Horizontal displacement between impulses | 3.00 in. |
| Vertical acceleration | 1.11 g/in. |
| Horizontal acceleration | 1.00 g/in. |

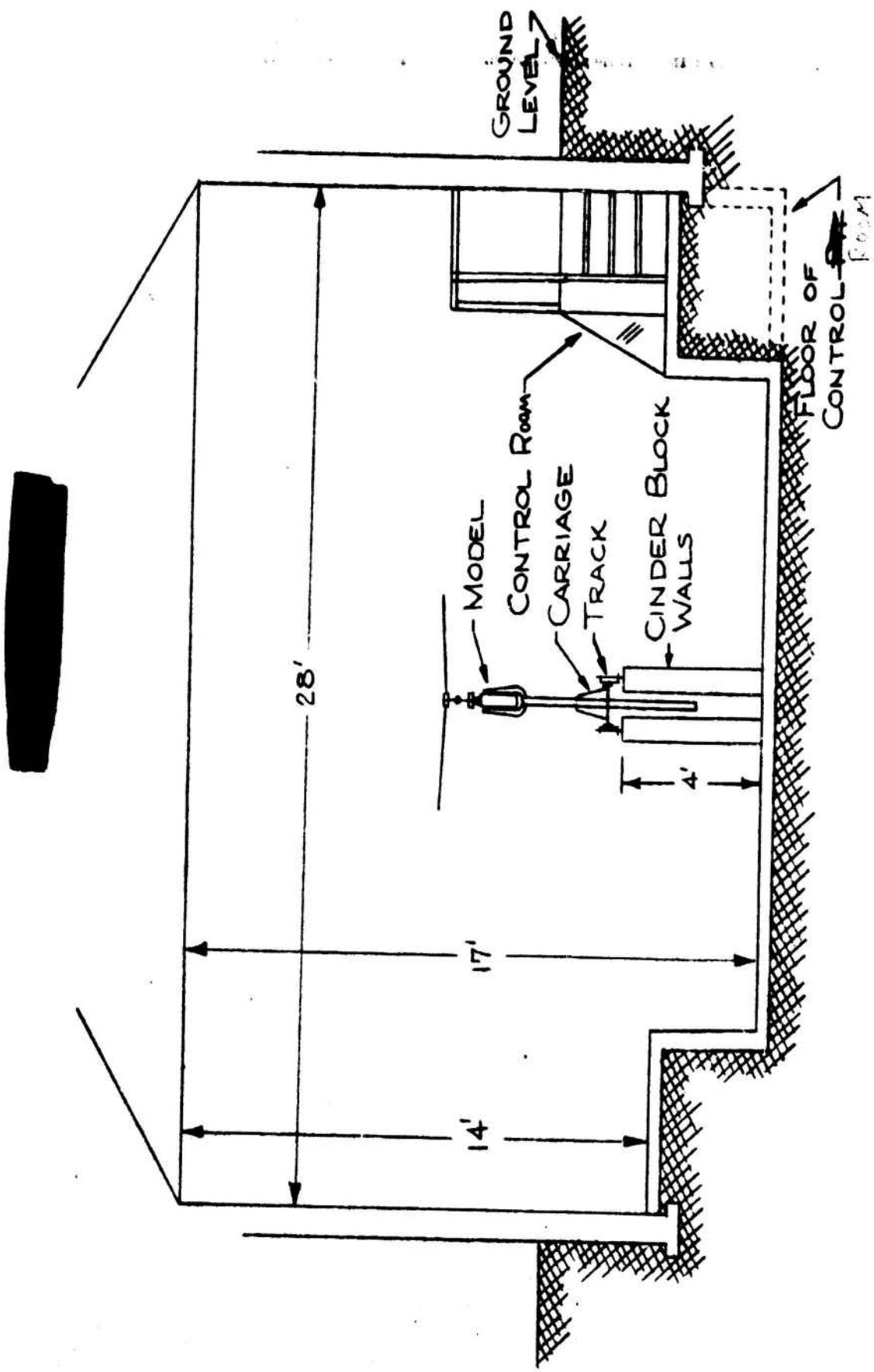


FIG. 1. CROSS SECTION OF HELICOPTER TEST SITE SHOWING MODEL IN FLIGHT POSITION

[redacted]

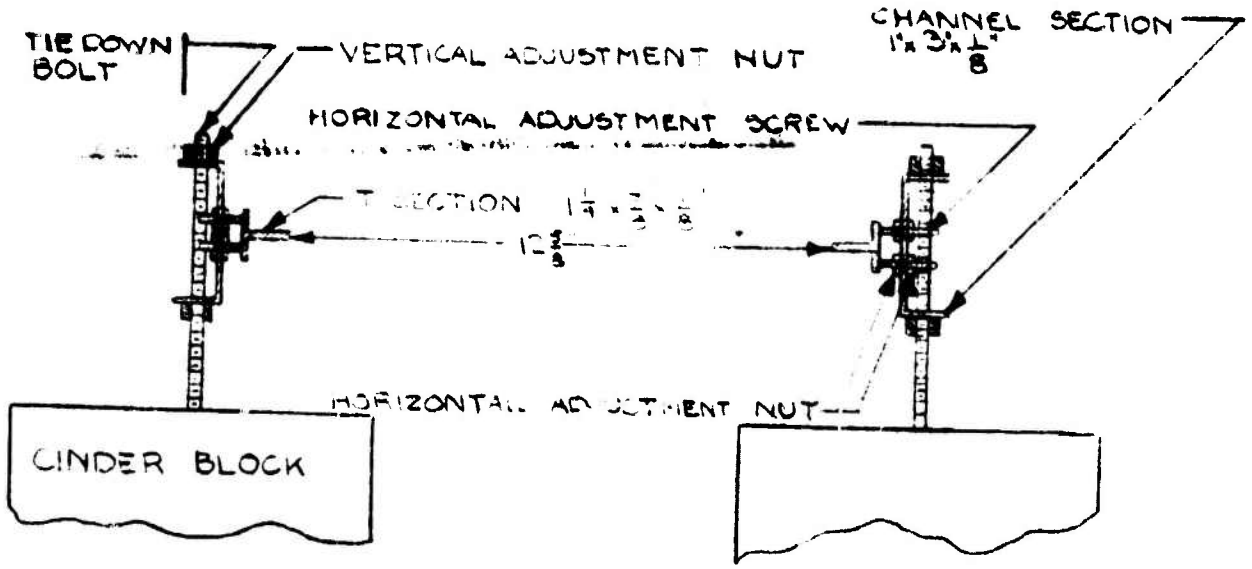


CROSS SECTION OF TRACK

FIGURE 2

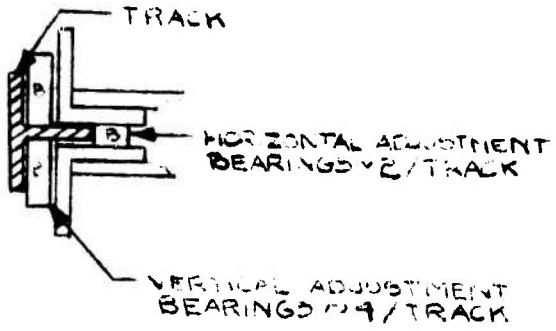


DETAIL OF TRACK BEARINGS

FIGURE 3

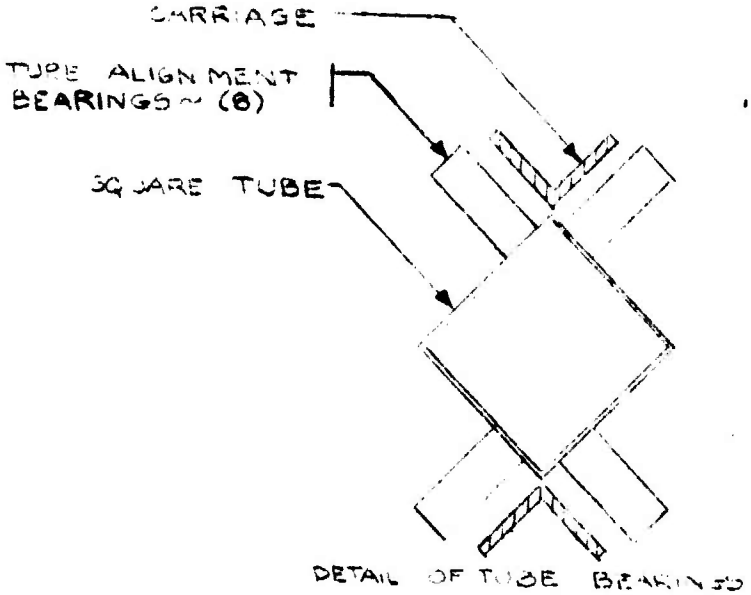


DETAIL OF TUBE BEARINGS

FIGURE 4

[redacted]

FIGURE 5 COMPLETELY DISASSEMBLED MODEL

FIGURE 6
FIRST ASSEMBLY STAGE

FIGURE 7
SECOND ASSEMBLY STAGE

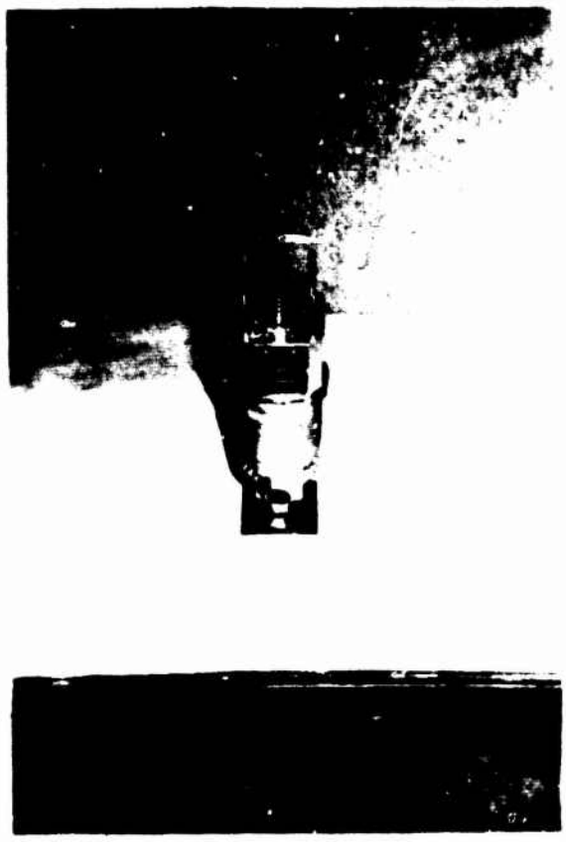

FIGURE 8
THIRD ASSEMBLY STAGE

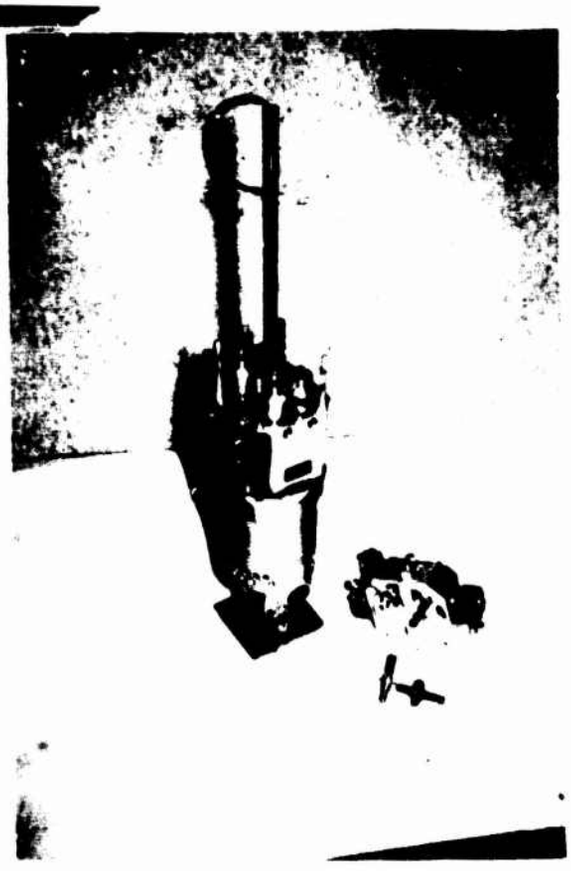

FIGURE 9
FOURTH ASSEMBLY STAGE

FIGURE 10
FIFTH ASSEMBLY STAGE

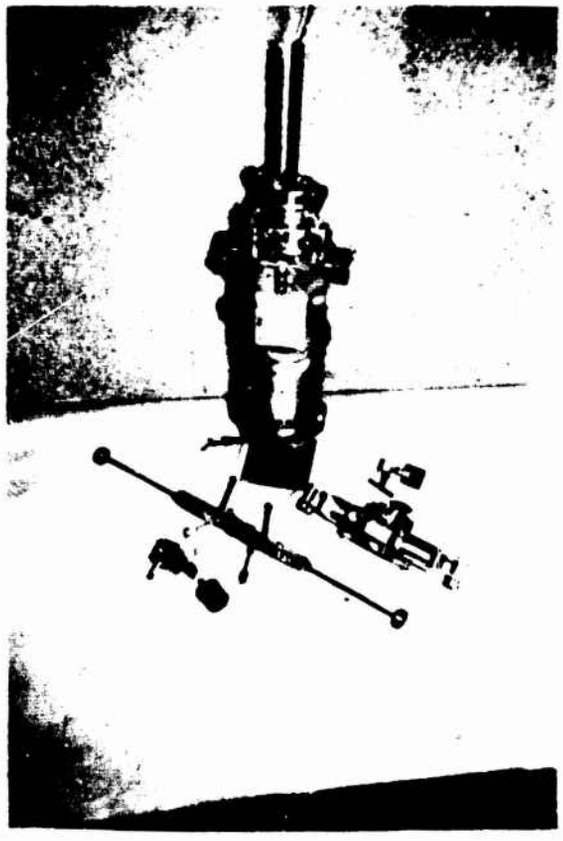

FIGURE 11
SIXTH ASSEMBLY STAGE

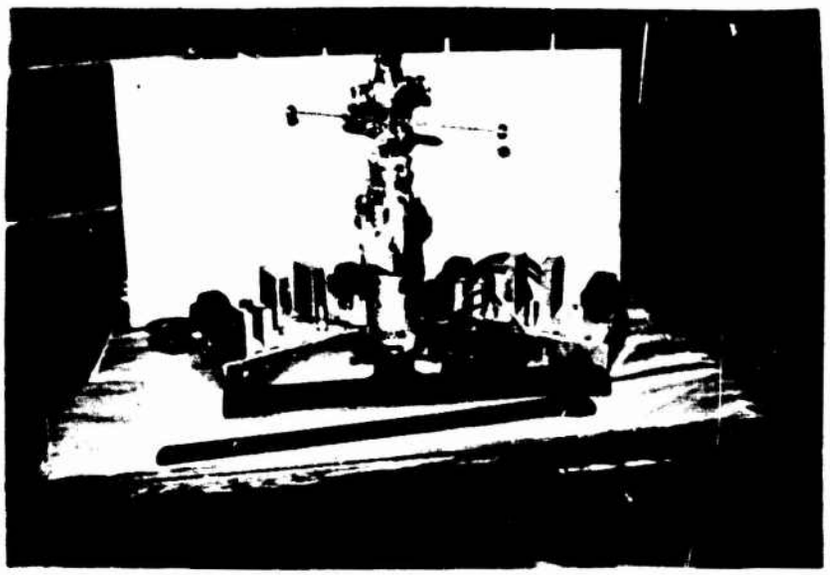

FIGURE 12 COMPLETELY ASSEMBLED MODEL WITH CLUTCH AMPLIFIERS, CONTROL BOX, AND BLADES

FIGURE 13 CLOSE-UP OF MODEL ROTOR SYSTEM

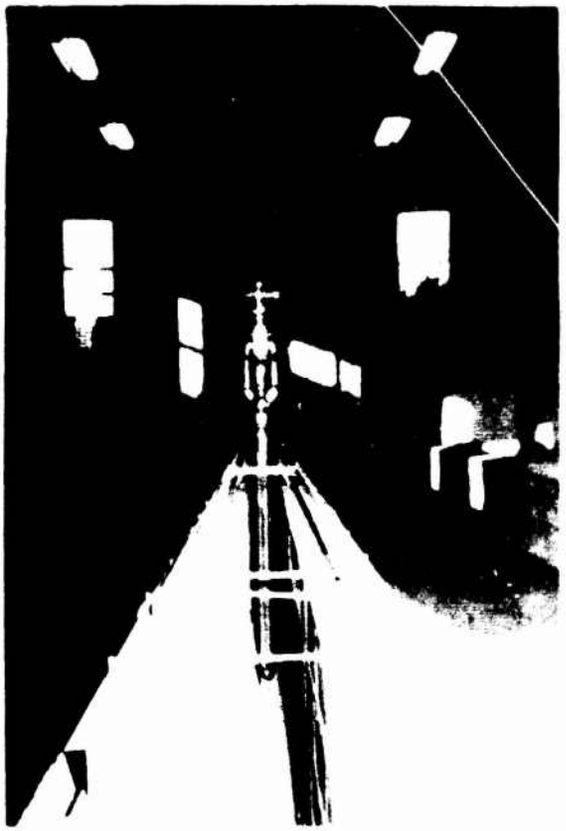

FIGURE 14 VIEW OF MODEL AND TRACK SYSTEM

FIGURE 15 VIEW OF MODEL MOUNTED IN YOKE AND ON CARRIAGE

FIGURE 16 GENERAL VIEW OF TEST LABORATORY

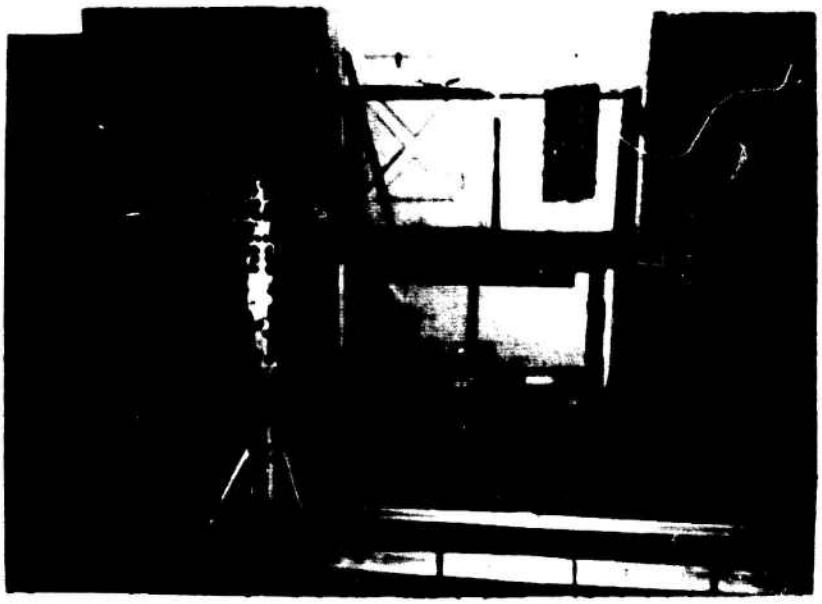

FIGURE 17 VIEW OF MODEL AND CONTROL ROOM

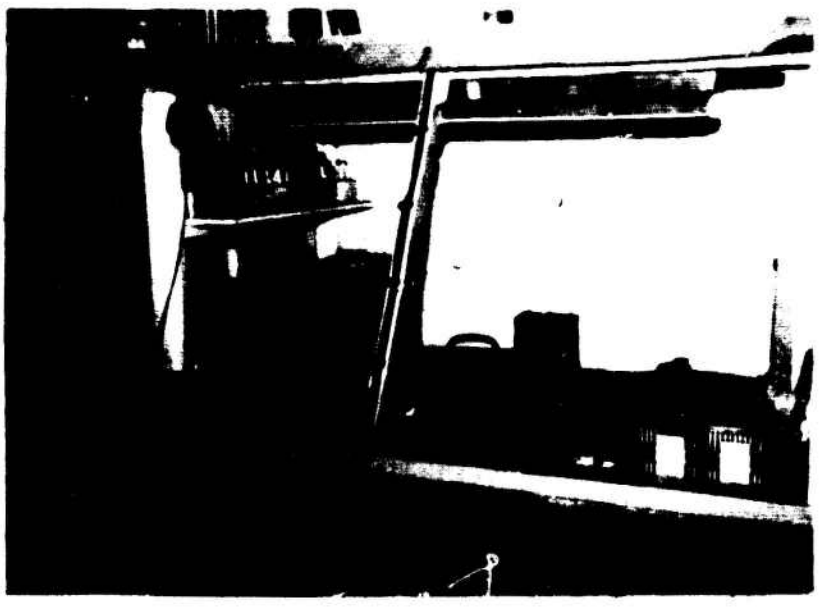

FIGURE 18 CLOSE-UP OF CONTROL ROOM

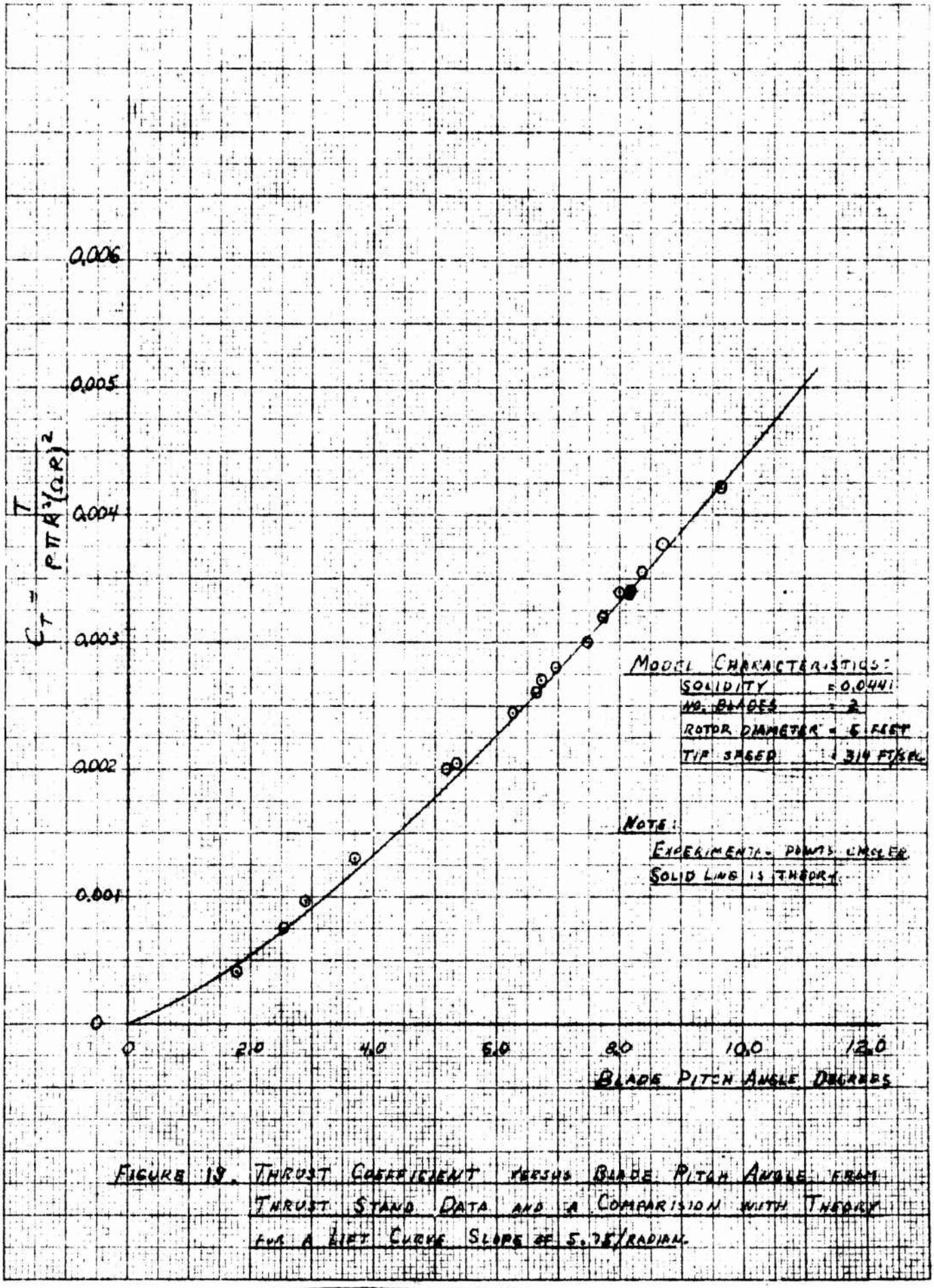


FIGURE 19. THRUST COEFFICIENT VERSUS BLADE PITCH ANGLE FROM THRUST STAND DATA AND A COMPARISION WITH THEORY FOR A LIFT CURVE SLOPE OF 5.73/RADIAN.

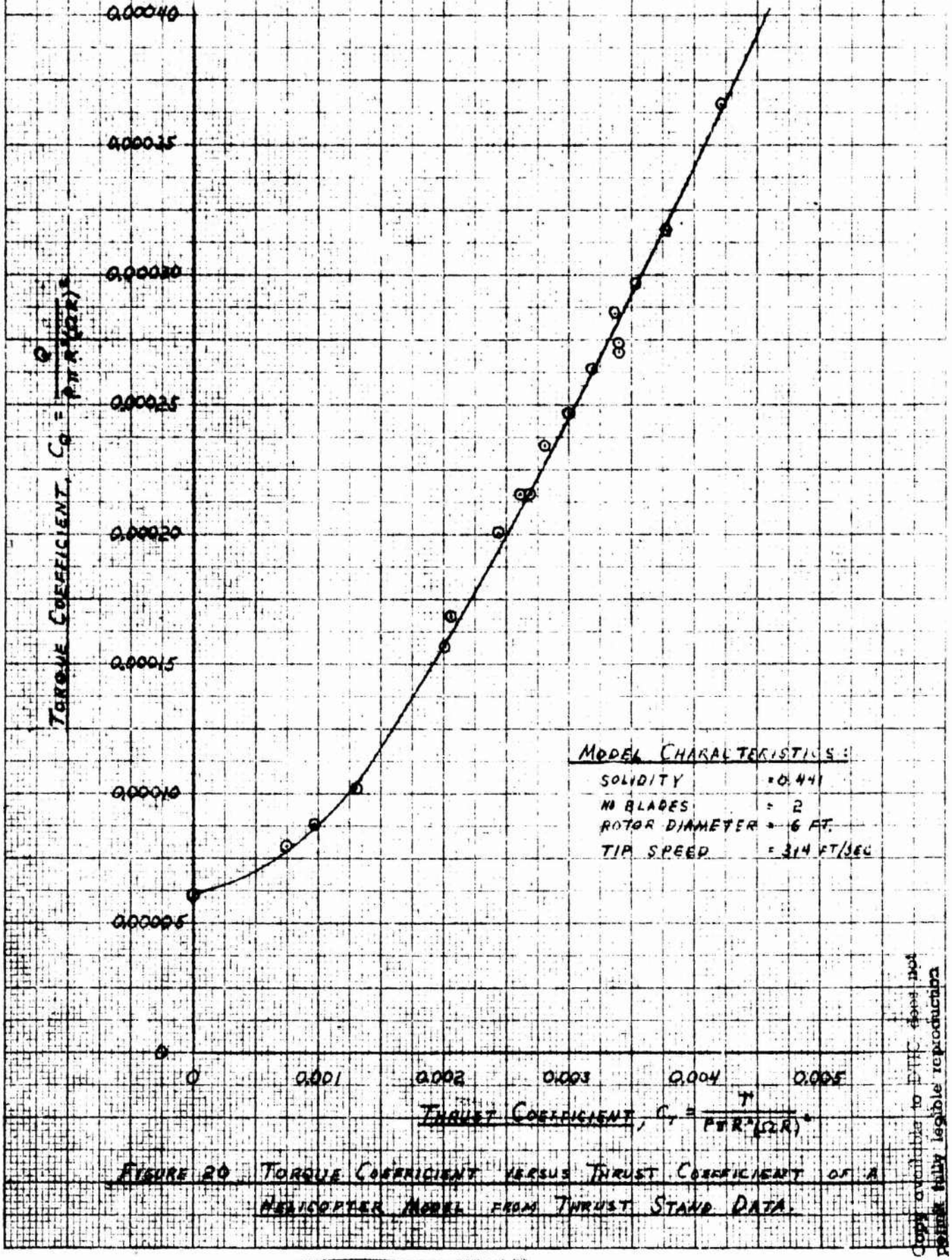


FIGURE 20 TORQUE COEFFICIENT VERSUS THRUST COEFFICIENT OF A HELICOPTER MODEL FROM THRUST STAND DATA.

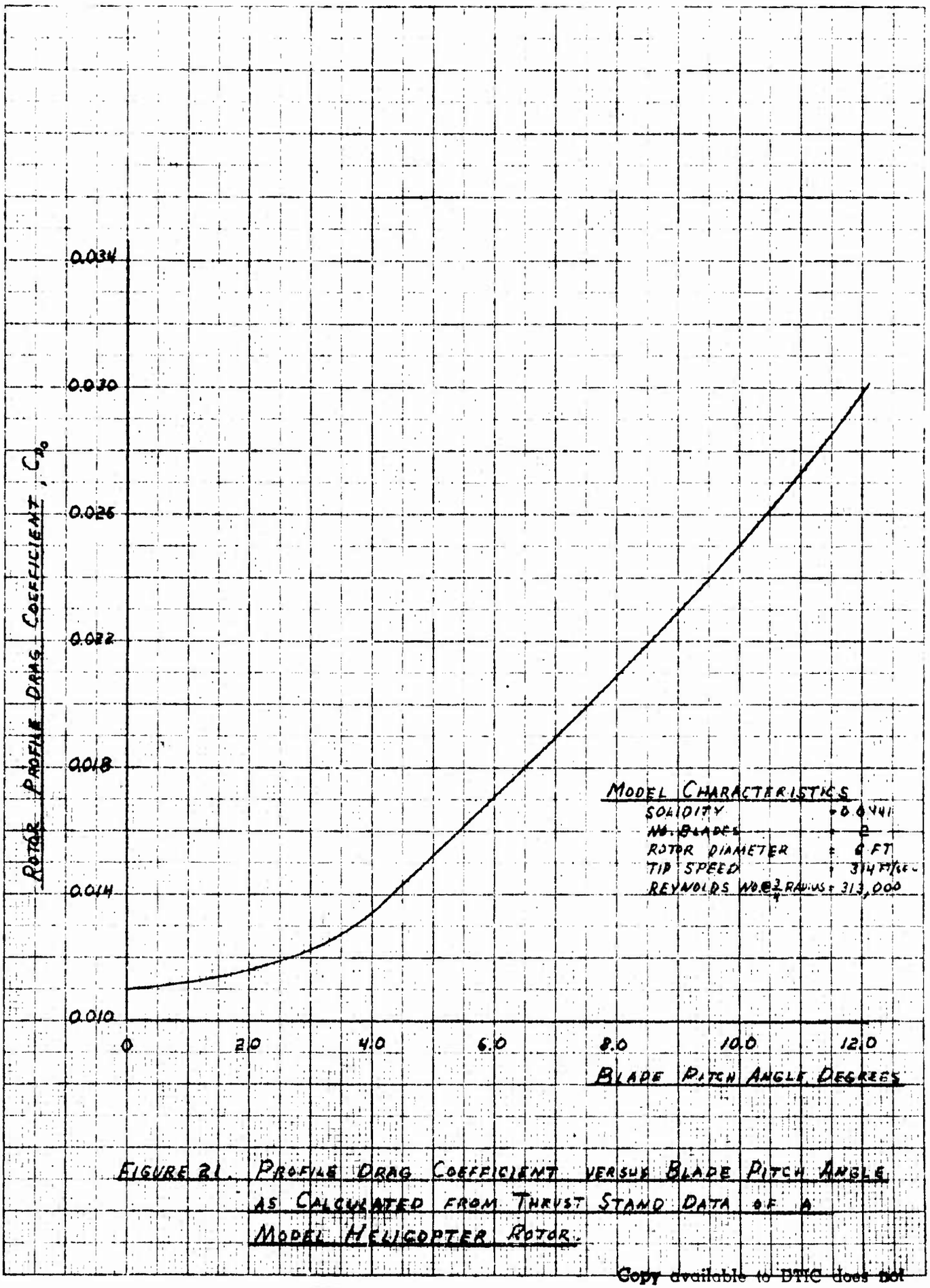


FIGURE 21. PROFILE DRAG COEFFICIENT VERSUS BLADE PITCH ANGLE AS CALCULATED FROM THRUST STAND DATA OF A MODEL HELICOPTER ROTOR.

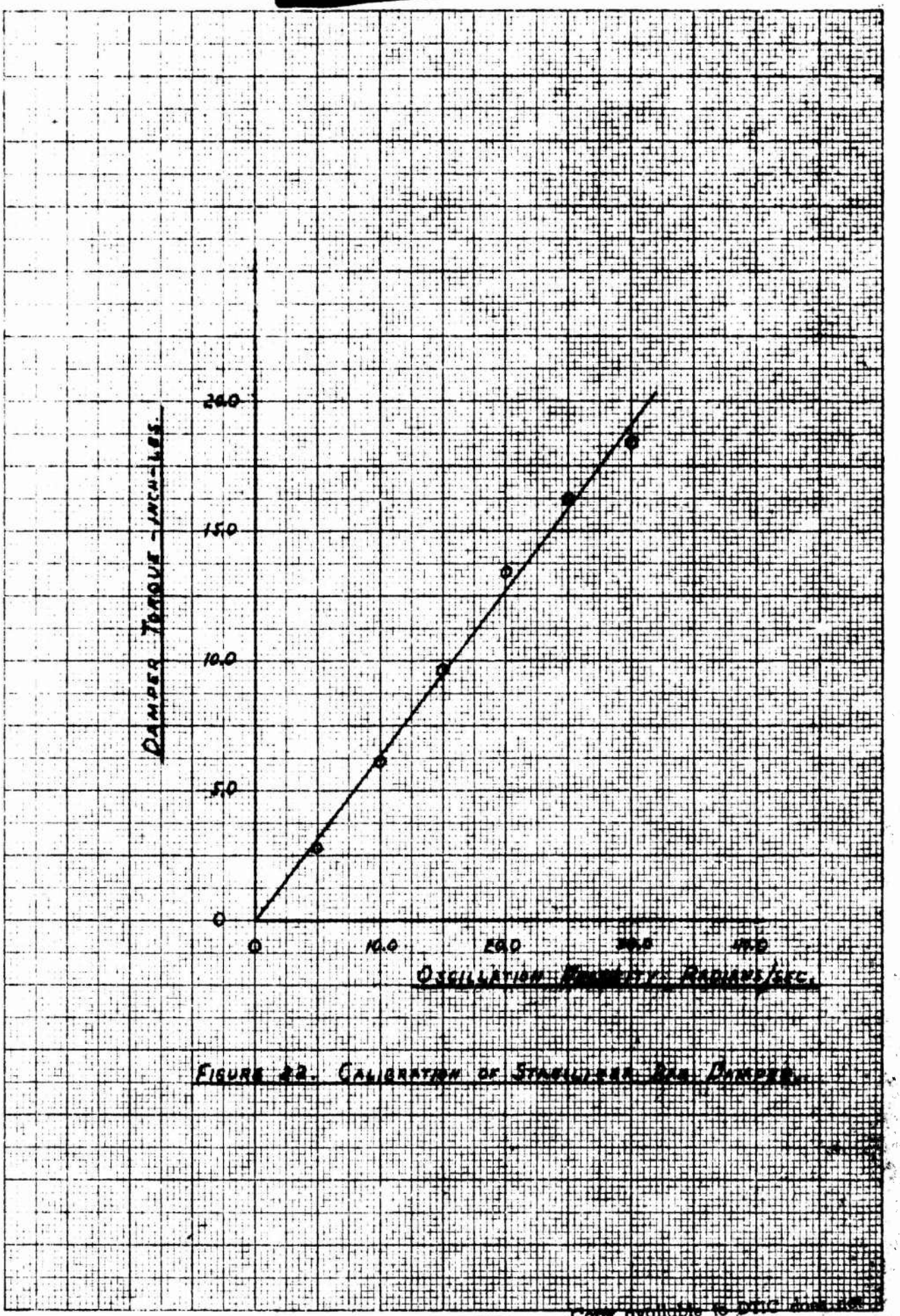


FIGURE 22. CALIBRATION OF STRAIN GAGE BAR DAMPER.

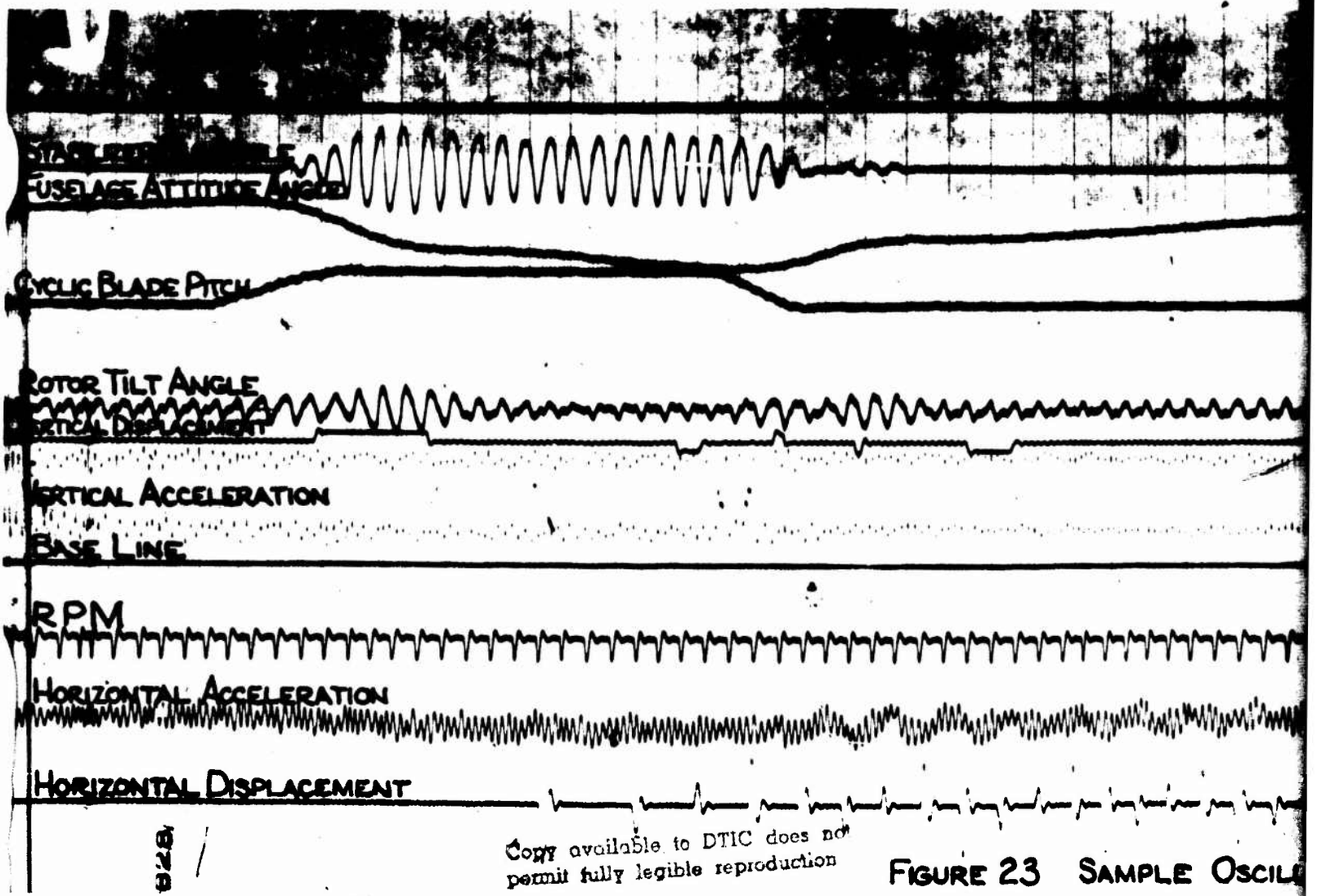




FIGURE 23 SAMPLE OSCIL

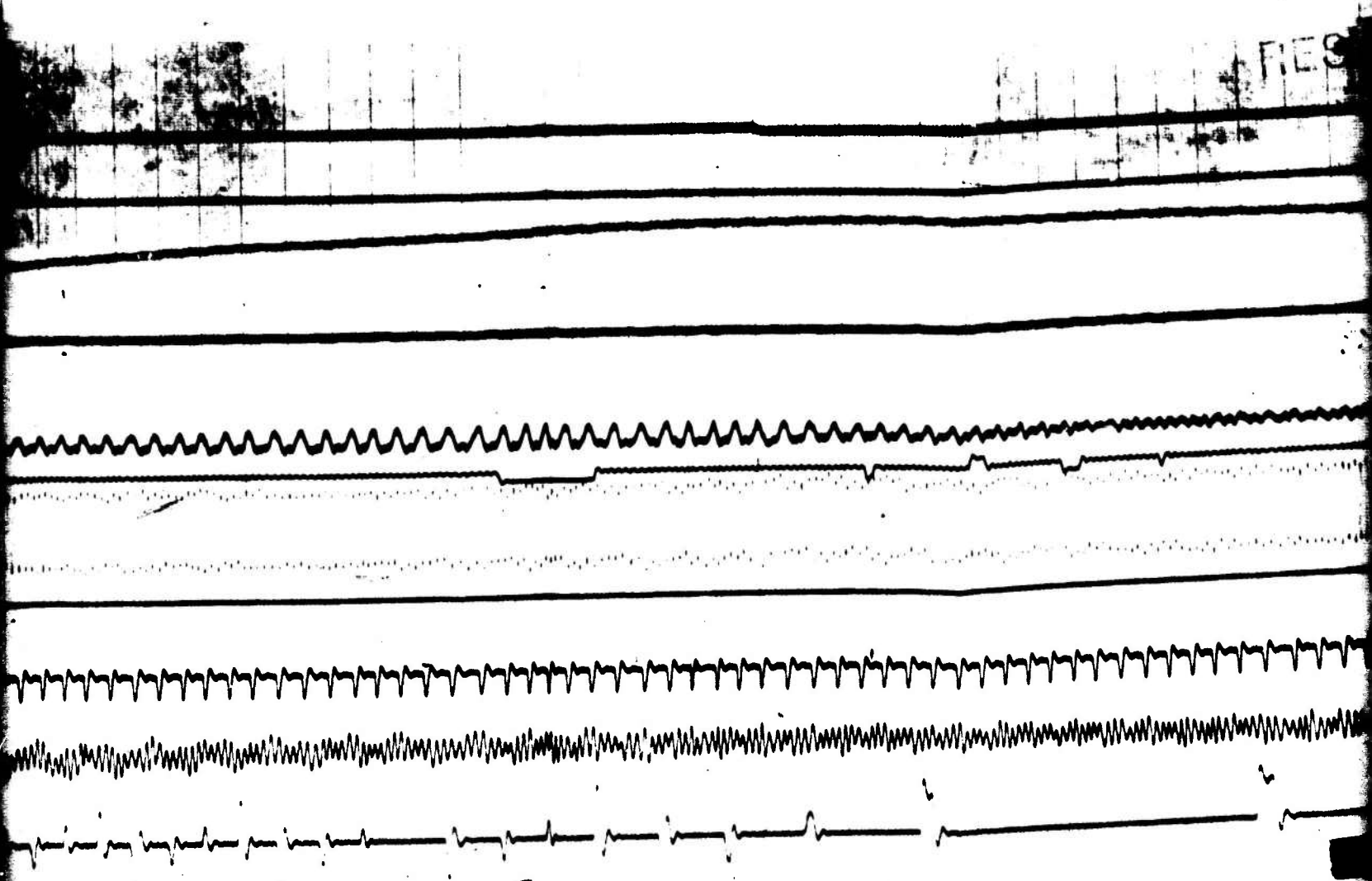

MPLE OSCILLOGRAPH RECORD 2

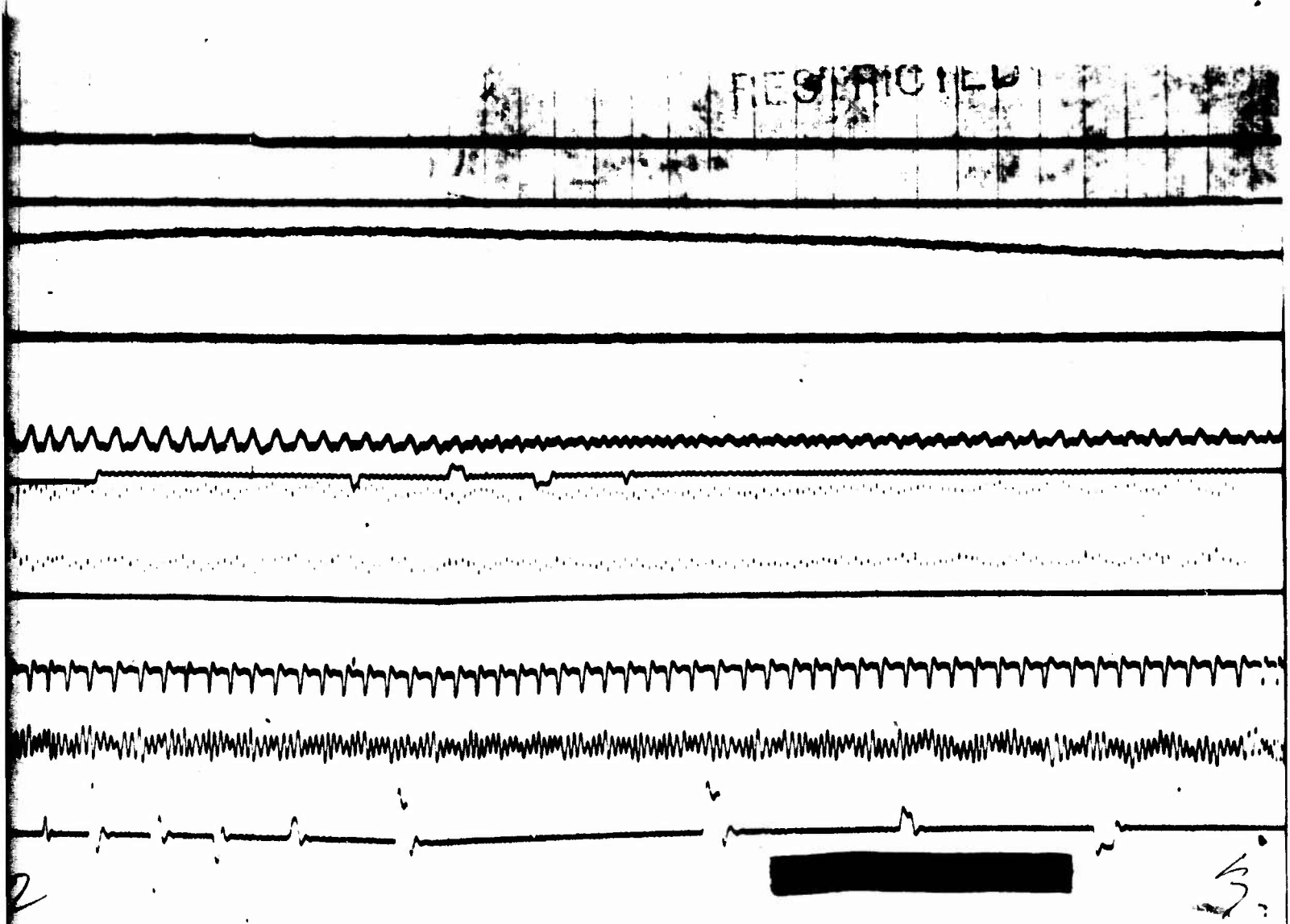
RESPIRATORY

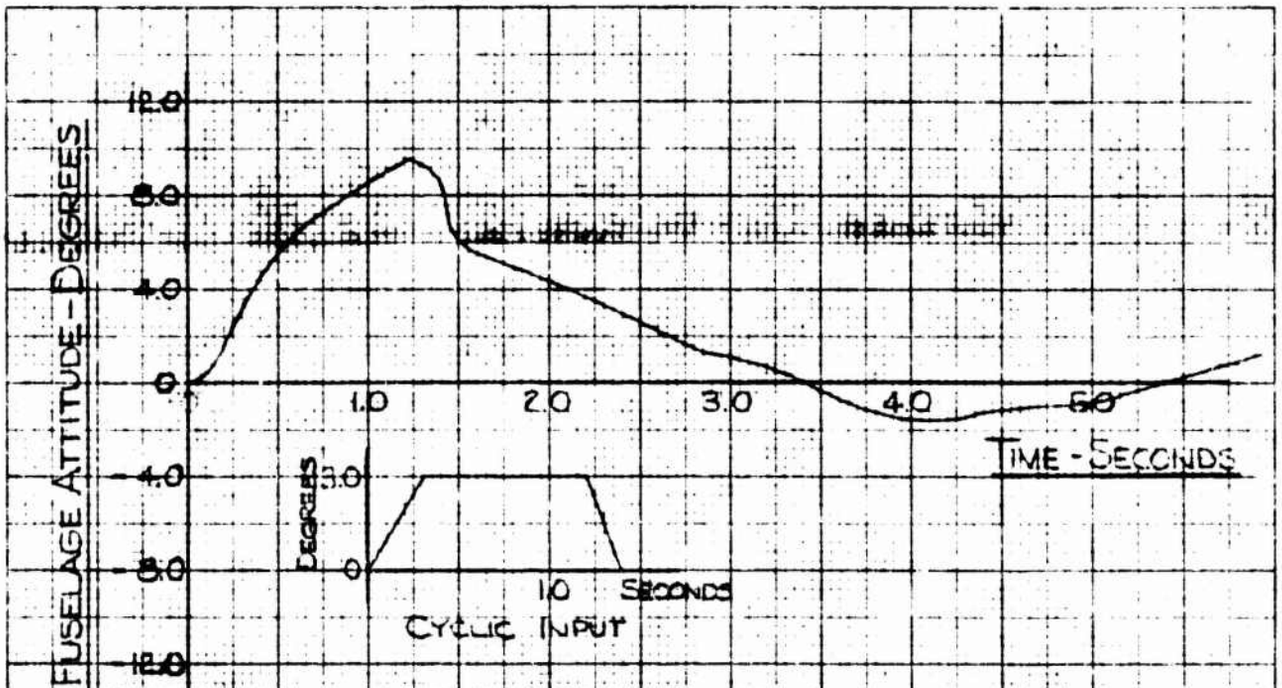


FIG. 24. EXPERIMENTAL FUSELAGE ATTITUDE RESPONSE TO GIVEN CYCLIC PITCH DISTURBANCE

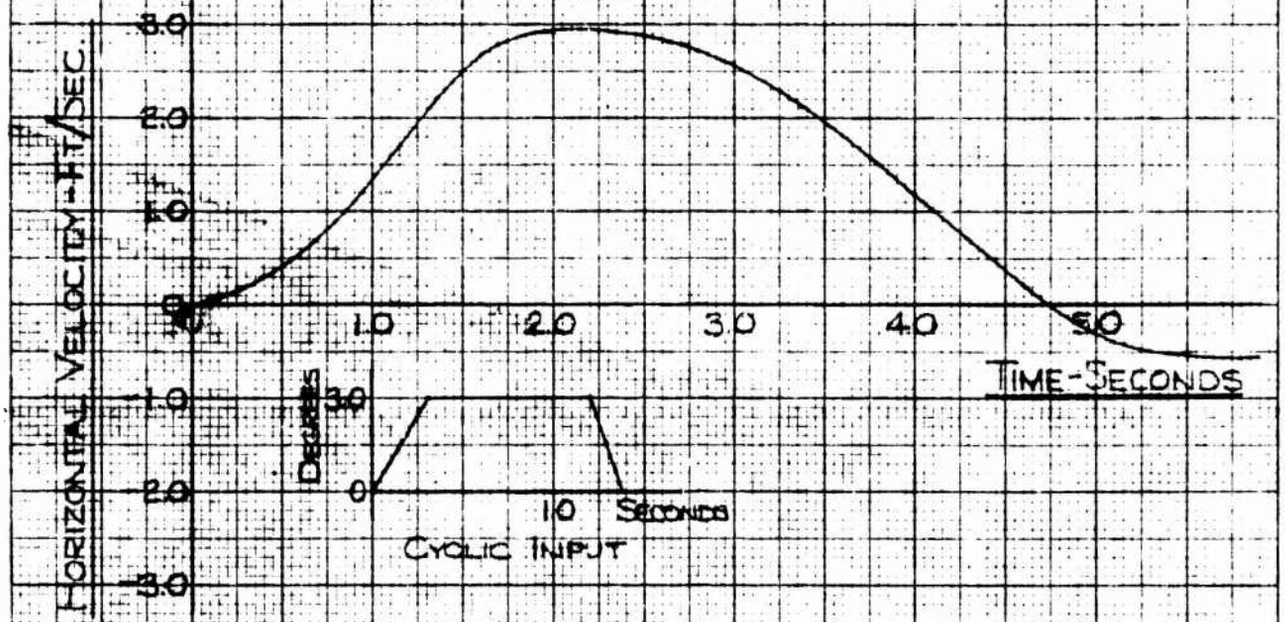


FIG. 25. EXPERIMENTAL HORIZONTAL VELOCITY RESPONSE TO GIVEN CYCLIC PITCH DISTURBANCE

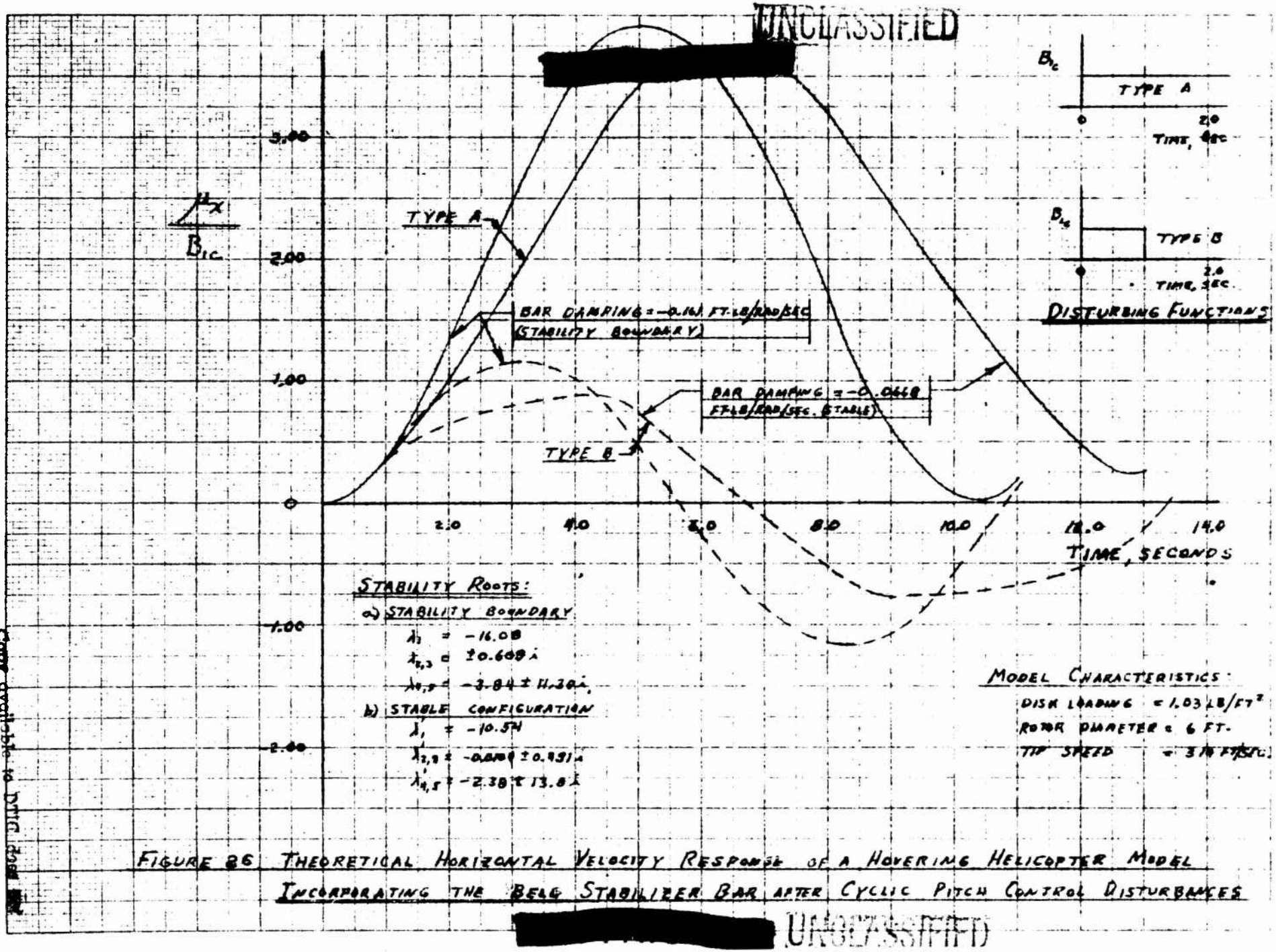


STABILITY ROOTS:

a) STABILITY BOUNDARY

$\lambda_1 = -16.08$

$\lambda_{2,3} = \pm 0.609\,i$

$\lambda_{4,5} = -3.84 \pm 11.20\,i$

b) STABLE CONFIGURATION

$\lambda'_1 = -10.54$

$\lambda'_{2,3} = -0.800 \pm 0.931\,i$

$\lambda'_{4,5} = -2.38 \pm 13.8\,i$

MODEL CHARACTERISTICS:

DISK LOADING = 1.03 LB/FT$^2$

ROTOR DIAMETER = 6 FT.

TIP SPEED = 316 FT/SEC.

FIGURE 26 THEORETICAL HORIZONTAL VELOCITY RESPONSE OF A HOVERING HELICOPTER MODEL INCORPORATING THE BELL STABILIZER BAR AFTER CYCLIC PITCH CONTROL DISTURBANCES

[redacted] UNCLASSIFIED

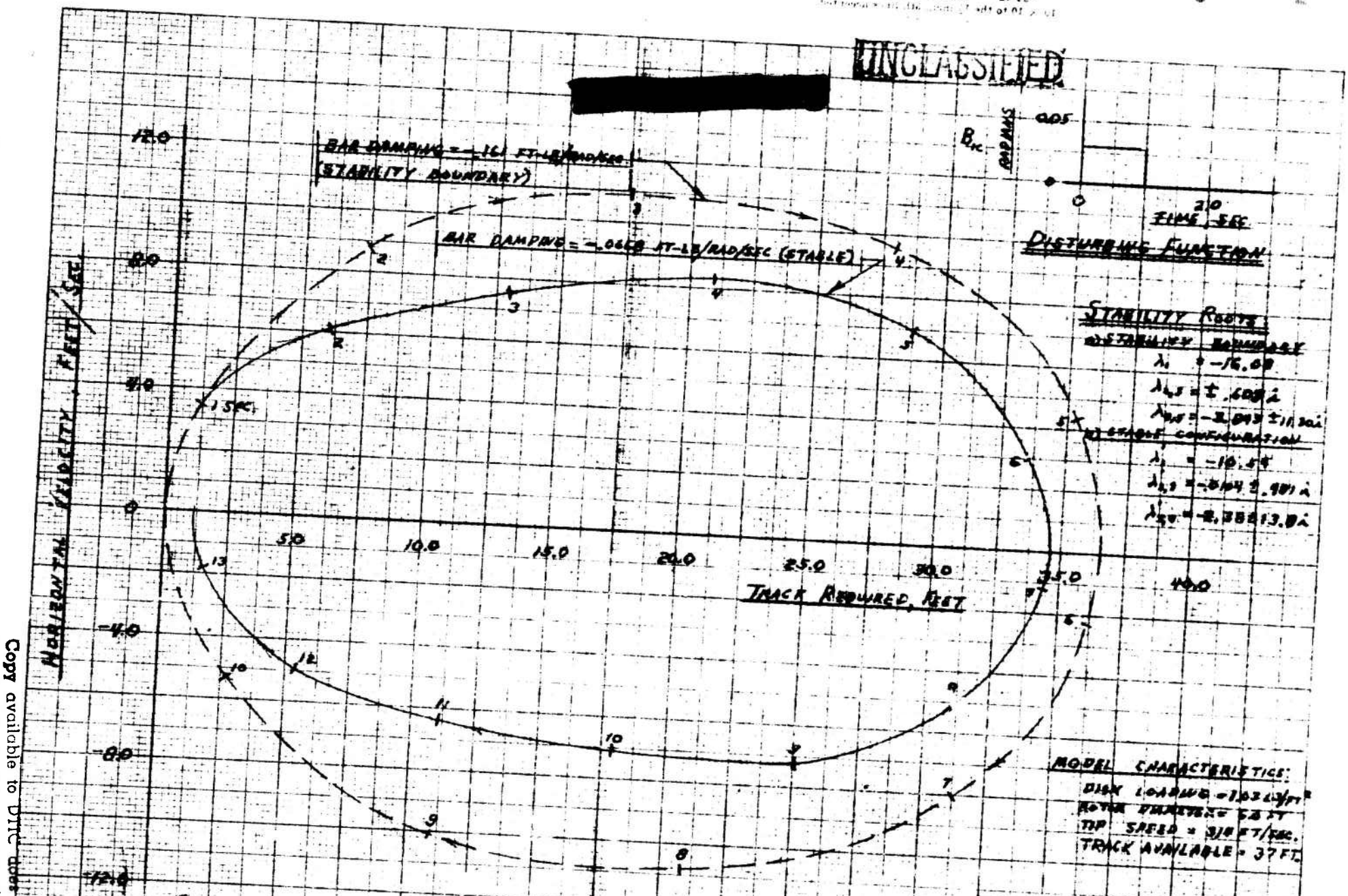


FIGURE 27. THEORETICAL HORIZONTAL VELOCITY RESPONSE OF A HOVERING HELICOPTER MODEL INCORPORATING THE [redacted] AFTER A CYCLIC PITCH CONTROL DISTURBANCE.

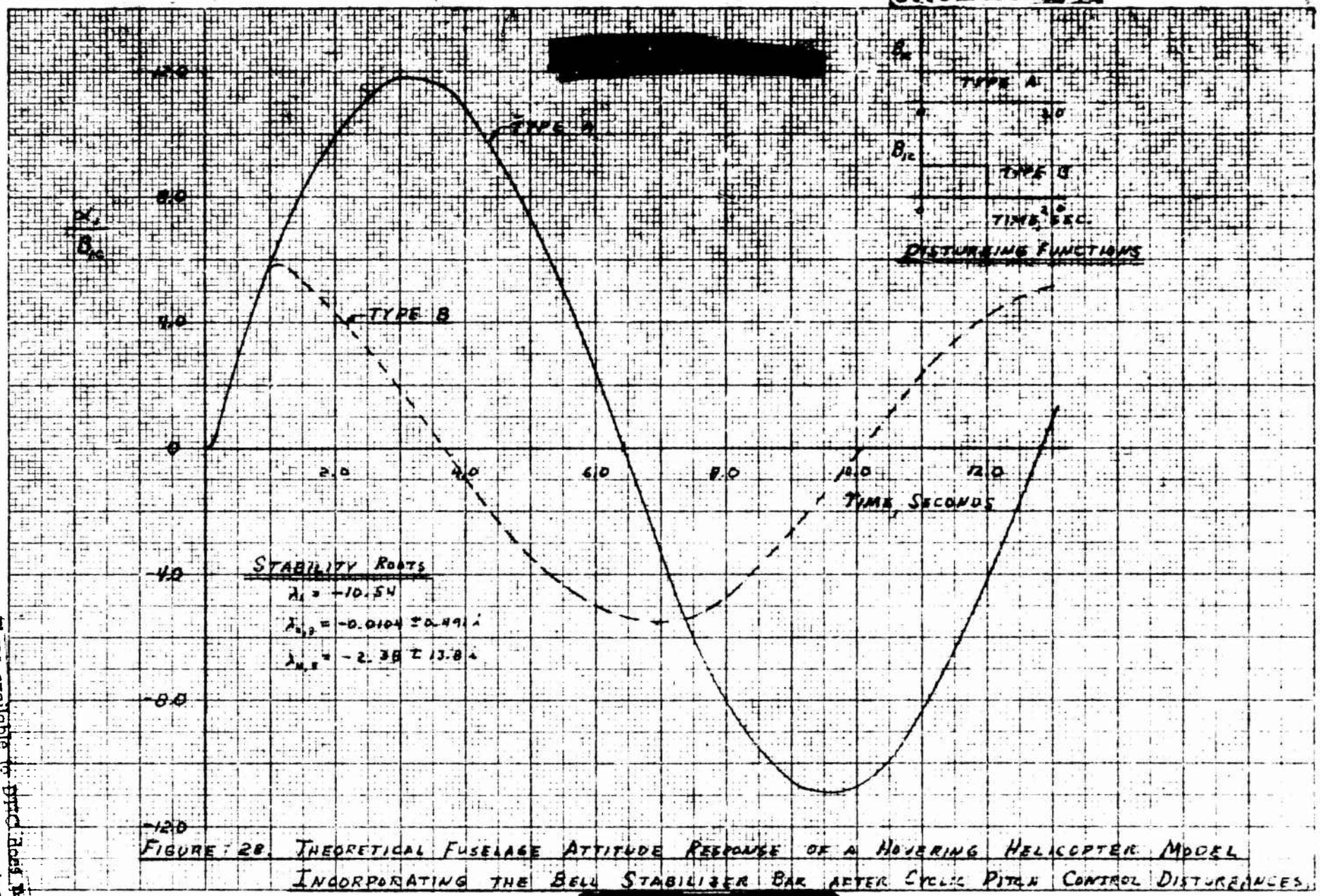


FIGURE 28. THEORETICAL FUSELAGE ATTITUDE RESPONSE OF A HOVERING HELICOPTER MODEL INCORPORATING THE BELL STABILIZER BAR AFTER CYCLIC PITCH CONTROL DISTURBANCES.